

Probing a dissipative phase transition via dynamical optical hysteresis

S.R.K. Rodriguez,^{1,*} W. Casteels,² F. Storme,² N. Carlon Zambon,¹ I. Sagnes,¹
L. Le Gratiet,¹ E. Galopin,¹ A. Lemaître,¹ A. Amo,¹ C. Ciuti,² and J. Bloch¹

¹*Centre de Nanosciences et de Nanotechnologies, CNRS, Univ. Paris-Sud,
Université Paris-Saclay, C2N—Marcoussis, 91460 Marcoussis, France*

²*Laboratoire Matériaux et Phénomènes Quantiques, Université Paris Diderot,
Sorbonne Paris Cité and CNRS, UMR 7162, 75205 Paris Cedex 13, France*

(Dated: February 9, 2017)

We experimentally explore the dynamic optical hysteresis of a semiconductor microcavity as a function of the sweep time. The hysteresis area exhibits a double power law decay due to the shot noise of the driving laser, which triggers switching between metastable states. Upon increasing the average photon number and approaching the thermodynamic limit, the double power law evolves into a single power law. This algebraic behavior characterizes a dissipative phase transition. Our findings are in good agreement with theoretical predictions, and the present experimental approach is promising for the exploration of critical phenomena in photonic lattices.

Optical bistability — the existence of two stable states with different photon numbers for the same driving conditions — is a general feature of driven nonlinear systems described within the mean-field approximation (MFA) [1]. Beyond the MFA, a quantum treatment predicts that the steady-state of a nonlinear cavity is unique at any driving condition [2]. The origin of this apparent contradiction was noted by Bonifacio and Lugiato [3], and by Drummond and Walls [4]: quantum fluctuations (the lost feature in the MFA) trigger switching between states and the exact solution corresponds to a weighted average over the two metastable states. Experiments in the 80's with two-mode lasers evidenced extremely long switching times [5], which were predicted to diverge for weak fluctuations and/or large photon numbers [6]. Already in these early works, this dramatic slowing down of the system dynamics was linked to a first order phase transition [5–7].

The physics of nonlinear resonators is receiving renewed interest in connection to predictions of quantum many-body phases [8–13], critical phenomena [5, 12–14, 16–18], and dissipative phase transitions [4]. Impressive progress is being made in building lattices of nonlinear resonators, such as photonic crystal cavities [20, 21], waveguides [22], superconducting microwave resonators [23, 24], or optomechanical resonators [25, 26]. In this context, semiconductor microcavities operating in the exciton-photon strong coupling regime provide a versatile platform where photon hopping and the pumping geometry can be controlled [27]. Lattices of different dimensionalities can be engineered [28, 29], and the hybrid light-matter nature of their elementary excitations, namely cavity polaritons, provide a strong and tunable Kerr nonlinearity via the exciton component [1, 30–32].

Recently, it was predicted that even in a single resonator, critical exponents could be retrieved from dynamical hysteresis measurements [17]. More precisely, when the driving power is swept at a finite speed across a bistability, the area of the hysteresis cycle is expected

to close following a double power-law as a function of the sweep time [5, 6]. The long-time decay arises from quantum fluctuations, and presents a universal -1 exponent [5]. In the thermodynamic limit wherein the photon number in the bistability tends to infinity and fluctuations are negligible, the algebraic decay of the hysteresis area is expected to evolve into a single power law [17]. This behavior characterizes a first order dissipative phase transition [17]. Exploring such dissipative phase transitions in a single cavity is a key step towards future studies with more complex systems.

In this Letter, we experimentally demonstrate the algebraic decay of the dynamical optical hysteresis in semiconductor micropillars. Scanning the power up and down at decreasing speeds, we observe the progressive closure of the hysteresis cycle induced by quantum fluctuations. The hysteresis area shows a double power-law decay as a function of the sweep time, with experimentally retrieved exponents in agreement with theoretical predictions. Probing different laser detunings and photon-photon interactions, we show that the algebraic decay evolves towards a single power law when the photon number becomes very large, i.e. when approaching the thermodynamic limit. Our results pave the way to the investigation of dissipative phase transitions in lattices of nonlinear resonators.

First, we briefly revisit the physics of a driven-dissipative single mode nonlinear cavity as illustrated in Fig. 5(a). ω_0 , γ , and U represent the mode frequency, loss rate, and photon-photon interaction strength (Kerr nonlinearity) of the cavity, driven by an electromagnetic field of frequency ω and intensity I . Within the rotating-wave approximation, the Hamiltonian (in units of $\hbar = 1$) is:

$$\hat{H}(t) = \omega_0 \hat{a}^\dagger \hat{a} + \frac{U}{2} \hat{a}^\dagger \hat{a}^\dagger \hat{a} \hat{a} + \sqrt{I} (e^{-i\omega t} \hat{a}^\dagger + e^{i\omega t} \hat{a}). \quad (1)$$

The boson operator \hat{a} (\hat{a}^\dagger) annihilates (creates) an exci-

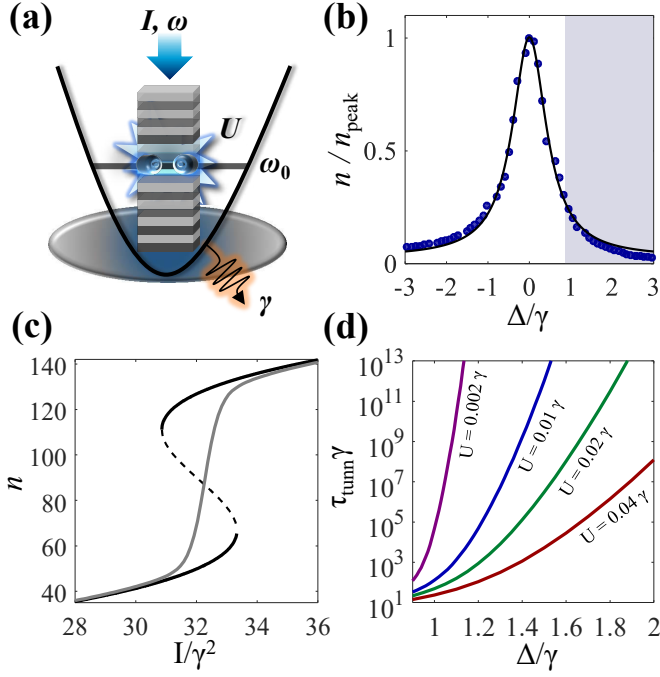


FIG. 1. (a) Sketch of a microcavity with mode frequency ω_0 , loss rate γ , photon-photon interactions of strength U , driven by an electromagnetic field of intensity I and frequency ω . (b) Normalized photon density in a semiconductor microcavity under weak driving. Experimental data points for the sample studied in Figs. 2, 3, and 4 are fitted with a Lorentzian lineshape. The shaded area indicates the mean-field bistable regime $\Delta \equiv \omega - \omega_0 > \sqrt{3}\gamma/2$ for $U > 0$. (c) Mean-field (black curves) and quantum (gray curves) solutions for a cavity with $U = 0.0075 \gamma$ probed at $\Delta = \gamma$. In the mean-field solution the solid and dashed curves are stable and unstable states, respectively. (d) Tunneling time τ_{tunn} between the two mean-field stable solutions.

tation in the resonator. The dynamics is described by the Lindblad master equation for the density matrix $\hat{\rho}(t)$:

$$\frac{\partial \hat{\rho}(t)}{\partial t} = i [\hat{\rho}, \hat{H}(t)] + \frac{\gamma}{2} (2\hat{a}\hat{\rho}\hat{a}^\dagger - \hat{a}^\dagger\hat{a}\hat{\rho} - \hat{\rho}\hat{a}^\dagger\hat{a}). \quad (2)$$

Equation 2 can be written as $\partial_t \hat{\rho} = \hat{\mathcal{L}} \hat{\rho}$, where $\hat{\mathcal{L}}$ is the Liouvillian superoperator. $\hat{\mathcal{L}}$ has a complex spectrum, of which two eigenvalues λ are particularly relevant for the long-time dynamics: i) $\lambda = 0$ corresponds to the steady-state, and ii) the non-zero eigenvalue with real part closest to zero is the Liouvillian gap $\bar{\lambda}$.

An exact expression for the steady-state photon density predicted by Eq. 2 was found in Ref. 4. This exact solution is shown as a gray line in Figure 5(c), for $U/\gamma = 0.0075$ and a laser-cavity detuning $\Delta = \omega - \omega_0 = \gamma$. The MFA follows from assuming the field to be coherent with amplitude $\alpha(t) = \langle \hat{a} \rangle$. Equation 2 then reduces to: $i \frac{\partial \alpha}{\partial t} = (\omega_0 - i\frac{\gamma}{2} + U|\alpha|^2) \alpha + \sqrt{I} e^{-i\omega t}$. The black line in Fig. 5(c) is the corresponding MFA calculation, display-

ing bistability for $31 < I/\gamma^2 < 33$. While the MFA implies a hysteresis cycle when varying the power across the bistability, the quantum solution is unique. This apparent contradiction is due to the absence of fluctuations in the MFA [3, 4]. Fluctuations (quantum or classical) render the mean-field steady-states metastable [3, 35], and the exact quantum solution corresponds to their average.

The reconciliation between numerous reports of optical bistability [31, 37–45] and the quantum prediction of a unique steady-state [4] follows from the fact that fluctuations can take astronomical times to induce switching between metastable states. Historically, this switching time is known as the tunneling time for bistability τ_{tunn} [46, 47], first-passage time [5], quantum activation time [48], or (inverse) asymptotic decay rate [4]. We will label this characteristic time as τ_{tunn} , which is the longest reaction time of the system given by the minimum value of $\bar{\lambda}$. Figure 5(d) shows τ_{tunn} as a function of Δ/γ for different U/γ . For weak interactions and/or large detunings, τ_{tunn} can vastly exceed realistic measurement times. Consequently, hysteresis measurements performed within a shorter time than τ_{tunn} lead to an apparent bistability. In this vein, Casteels and co-workers predicted how the hysteresis area should be influenced by quantum fluctuations when the scanning time across the “bistability” is commensurate with τ_{tunn} [5]. In particular, they predicted double power-law decay of the hysteresis area [5], in contrast with previous reports of a single power-law decay [39].

To measure dynamic optical hysteresis, we use rectangular micropillars etched from a GaAs λ planar cavity containing one 8 nm $\text{In}_{0.04}\text{Ga}_{0.96}\text{As}$ quantum well and surrounded by two $\text{Ga}_{0.9}\text{Al}_{0.1}\text{As}/\text{Ga}_{0.05}\text{Al}_{0.95}\text{As}$ distributed Bragg reflectors with 26 and 30 pairs of layers at the top and bottom, respectively. The sample is maintained at 4 K and driven by a frequency-tunable single-mode laser. We probe the lowest energy mode of the micropillars, whose linewidth ranges from 28 to 34 μeV [49]. The value of U is estimated from the energy of the confined polariton mode and its exciton fraction [49]. The laser power is modulated by an electro-optic modulator (EOM) fed by a waveform generator [see Figure 2(a)]. The waveform contains a series of ~ 50 triangular ramps of variable time-duration. The transmission through the cavity is measured with a photodiode connected to an oscilloscope. The scanning times t_s (the time it takes to ramp the power from the lowest to the highest value) span the 0.8–50 kHz range. As shown in the supplemental information, laser shot noise is the only noise source within this frequency range and we exclude additional fluctuations from our observations [49].

We are interested in the hysteresis area,

$$A = \int_{P_{\min}}^{P_{\max}} |n_{\downarrow}(P) - n_{\uparrow}(P)| dP, \quad (3)$$

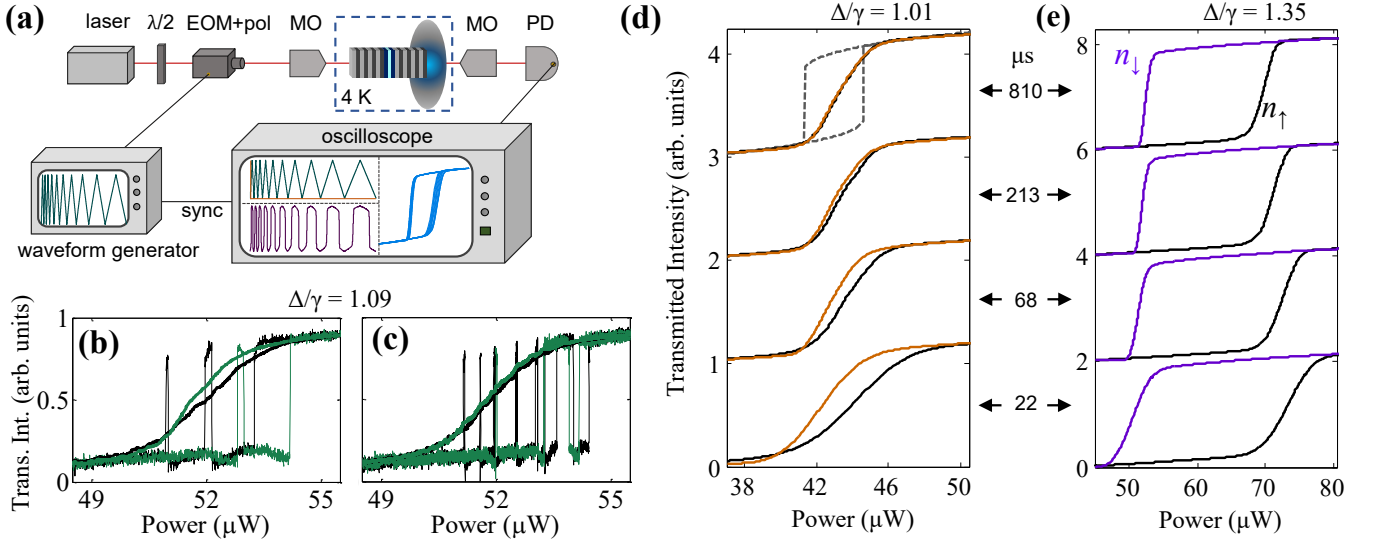


FIG. 2. (a) Experimental setup: $\lambda/2$, MO, PD, and EOM+pol, stand for half-wave plate, microscope objective, photodiode, and electro-optic modulator with a polarizer, respectively. The green (purple) traces in the waveform generator and in the oscilloscope are measurements of the incident (transmitted) signals. The hysteresis cycles in the oscilloscope are obtained by plotting the transmitted versus the incident signal, overlaid for various scanning times. The colored and black lines in (b)-(e) represent the transmission when the power is ramped down and up, respectively. (b) and (c) show single shot (thin lines) and averages over 1000 realizations (thick lines) of dynamic hysteresis. The scanning time is $t_s = 0.11$ ms in (b), and $t_s = 0.43$ ms in (c). (d) and (e) show dynamic hysteresis averaged over 1500 realizations. The dashed line in (d) is the mean-field calculation corresponding to the experiment.

as a function of t_s . $n_\downarrow(P)$ and $n_\uparrow(P)$ represent the cavity transmission when the power is ramped down and up, respectively. P_{\min} and P_{\max} are powers below and above the hysteresis range. In the absence of fluctuations, A saturates to a finite value (the mean-field static hysteresis area) for $t_s \rightarrow \infty$ [39]. However, unavoidable quantum fluctuations induce spontaneous switchings between the mean-field “bistable” states. Consequently, the hysteresis area averaged over many realizations, A_{av} , is expected to close in proportion to the number of switching events, such that $\lim_{t_s \rightarrow \infty} A_{\text{av}} = 0$.

In Figs. 2(b, c) we compare single-shot (thin lines) and averaged (thick lines, 1000 realizations) transmission measurements for $\Delta/\gamma = 1.09$. The single-shot measurements in Fig. 2(c) display more switchings than in Fig. 2(b) because the sweep is slower in Fig. 2(c). Consequently, the average hysteresis area in Fig. 2(c) is reduced.

Figure 2(d) show hysteresis measurements (averaged over 1500 realizations) for $\Delta/\gamma = 1.01$ and different values of t_s . The hysteresis area close for increasing t_s . For the slowest sweep, the measured cycle strongly deviates from the mean-field prediction (dashed lines) and resembles the exact quantum prediction in Fig. 5(c). In contrast, for larger Δ/γ , $\tau_{\text{tunn}} \gg t_s$ and the hysteresis area changes marginally [see Fig. 2(e)].

The behavior of A_{av} not only depends on t_s , but also on the scanned power range $P_s \equiv P_{\max} - P_{\min}$. The ratio t_s/P_s gives an effective (inverse) sweep speed. In

Fig. 3(a) we plot A_{av} as a function of t_s/P_s for 6 different Δ/γ . For small Δ/γ we observe two power laws indicated by the gray and blue lines in Fig. 3(a). The blue lines correspond to a power-law with a -1 exponent, as predicted in Ref. 5. This is the regime dominated by quantum fluctuations, when $\tau_{\text{tunn}} < t_s$. For increasing Δ/γ , the average photon number in the bistability increases and fluctuations become relatively weaker. Consequently, the -1 power law sets in at longer times and A_{av} follows a single power law within the experimental observation window.

Calculating the dynamics behind the results in Fig. 3(a) requires a time-evolution up to 10^8 times the polariton lifetime (21 ps), a temporal resolution below the polariton lifetime, and a dimensionality of the Hilbert space of $\sim 10^3$. To circumvent this difficulty, Ref. 5 introduced a method based on a scaling analysis in the spirit of the Kibble-Zurek mechanism for dynamic phase transitions [50]. The key idea is that a power sweep at a finite rate across the bistability involves a non-adiabatic response of the system, resulting in the dynamic hysteresis. The non-adiabatic intensity range δI is determined by comparing the sweep time scale τ_S with the system reaction time τ_R (see Fig. 3 (b) inset and supplementary information [49]). The longest reaction time is τ_{tunn} . Similar to the hysteresis area A_{av} , δI exhibits a double power-law as a function of the sweep rate [5].

Figure 3(b) shows calculations of δI reproducing our experimental observations. The lines in Fig. 3(b) all have

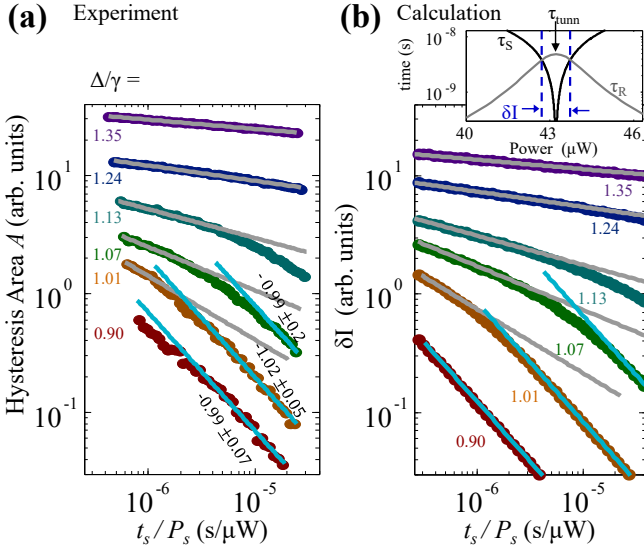


FIG. 3. (a) Measured hysteresis area A_{av} (defined in Eq. 3) as a function of t_s/P_s , where P_s is the scanned power range. Different colors correspond to different values of Δ/γ . The gray lines are power law fits with an exponent greater than -1. The blue lines indicate power laws in the regime influenced by quantum fluctuations. The experimentally retrieved exponents in this regime are shown with 2σ confidence intervals on the fits. (b) Calculations of the non-adiabatic range δI of the driving intensity using the scaling analysis described in the text. The power laws in (b) all have the same exponents retrieved from the fits in (a). The inset in (b) shows the system reaction time τ_R in gray, and the sweep time scale τ_s in black, for $U = 0.0075 \gamma$ and $\Delta = 1.01 \gamma$. The dashed blue lines indicate the non-adiabatic range δI . The conversion of the theoretical intensity units to the experimental power units is described in the supplemental information [49].

slopes deduced from the power law fits to the measurements in Fig. 3(a). A good agreement between measurements and calculations is obtained for every Δ/γ . This confirms the exponents expected for a single mode cavity under the influence of quantum fluctuations. To obtain this good agreement, we adjusted the value of U/γ within the experimental uncertainty. We take $U/\gamma = 7.5 \cdot 10^{-3}$, whereas the experimental estimate [49] is $U/\gamma = 2 \cdot 10^{-3} {}^{+8 \cdot 10^{-3}}_{-1.6 \cdot 10^{-3}}$. Overall, the results in Fig. 3 show that as Δ/γ decreases and the photon number in the bistability decreases, the hysteresis area evolves from a single to a double power law decay. This transition is due to the influence of quantum fluctuations.

A thermodynamic limit can be defined for a single resonator by letting $N \rightarrow \infty$ and $U \rightarrow 0$ while keeping $U \cdot N$ constant [17]. This limit can be explored probing cavities with different values of U/γ at a fixed laser-cavity detuning Δ/γ . Experimentally, we vary U/γ by selecting micropillars with different lateral dimensions. A reduced cross-sectional area of the micropillar blue-shifts the energy of the confined polariton modes and increases their exciton fraction, thereby increasing U/γ [49]. Figure 4(a)

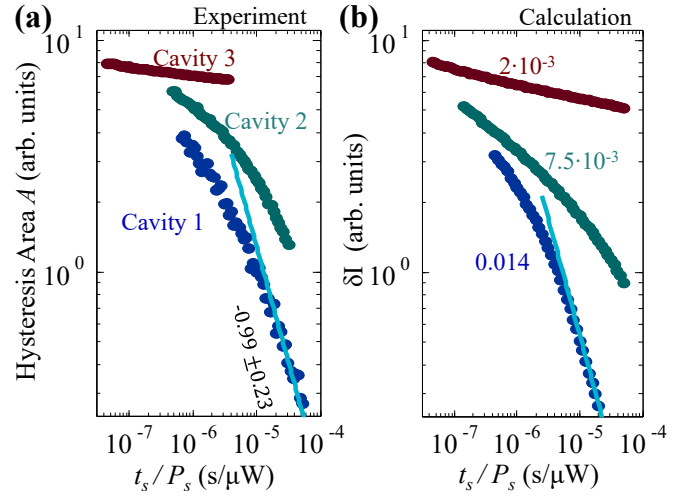


FIG. 4. (a) Measurements of the hysteresis area A for three cavities with different U/γ and approximately equal Δ/γ . U/γ decreases from cavity 1 to cavity 3. (b) Calculations of δI as explained in the text and in Fig. 3. For the highest and lowest curves $\Delta/\gamma = 1.15 \pm 0.1$, while for middle curve $\Delta/\gamma = 1.13 \pm 0.1$, both in experiments and calculations. In (a), the curve corresponding to cavity 3 was divided by 80. In (b), the curve corresponding to the smallest U/γ was divided by 4, and the curve corresponding to the largest U/γ was multiplied by 2. These multiplications (for improving visibility) only shift the curves vertically and do not change the exponent.

shows measurements of A_{av} for three cavities probed at $\Delta/\gamma = 1.15 \pm 0.1$. For cavity 1 with the strongest interaction strength, A_{av} displays a double power law with the -1 exponent at large t_s/P_s . As U/γ decreases, the time at which the power law with the -1 exponent sets in increases. For cavity 3 with the weakest interaction strength, A_{av} depends marginally on t_s/P_s and the data follows a single power law. These observations are consistent with the dramatic dependence of τ_{tunn} on U/γ plotted in Fig. 5(d).

Figure 4(b) shows calculations based on the scaling analysis previously described, in good agreement with the measurements in Fig. 4(a). Details about the values of U/γ used in the calculations are discussed in the supplemental information [49]. Overall, Fig. 4 demonstrates that as $U \rightarrow 0$ and the average photon number in the bistability increases, the hysteresis area evolves towards a single power-law decay. This is the signature of a system approaching the thermodynamic limit of high photon numbers [17].

To summarize, we showed a double power-law decay of the hysteresis area as a function of the sweep rate. As the average photon number increases and quantum fluctuations become relatively weaker, the tunneling time increases dramatically. This shifts the transition in the power law with exponent -1 to larger times. In the thermodynamic limit of large photon numbers, the hystere-

sis area exhibits a single power-law decay. These results open the way to the exploration of dissipative phase transitions in lattices of coupled micropillars, where photon hopping can give rise to intriguing behavior. For instance, a square lattice of bistable resonators has been mapped to an equilibrium Ising model with an effective temperature given by the losses [18]. The question remains open regarding phase transitions in more elaborate lattices with intricate topologies [51], with spin-orbit coupling [52], or with quasi-crystalline structure [53] in which thermodynamic properties reflect their non-integer dimensions [54, 55].

This work was supported by the Marie Curie individual fellowship PINQUAR (Project No. 657042), the French National Research Agency (ANR) program Labex NanoSaclay via the projects Qeage (ANR-11-IDEX-0003-02) and ICQOQS (ANR-10-LABX-0035), the French RENATECH network, the ERC grant Hon-eypol and the EU-FET Proactiv grant AQUUS (Project No. 640800). W.C., F. S., and C.C. acknowledge support from ERC (via the Consolidator Grant "CORPHO" No. 616233).

* said.rodriquez@lpn.cnrs.fr

- [1] H.M. Gibbs, *Optical Bistability: Controlling Light with Light*, Quantum Electronics Series (Academic Press, 1985).
- [2] D.F. Walls and G.J. Milburn, *Quantum Optics*, Springer-Link: Springer e-Books (Springer Berlin Heidelberg, 2008).
- [3] R. Bonifacio and L. A. Lugiato, "Photon statistics and spectrum of transmitted light in optical bistability," *Phys. Rev. Lett.* **40**, 1023–1027 (1978).
- [4] P. D. Drummond and D. F. Walls, "Quantum theory of optical bistability. I. Nonlinear polarisability model," *J. Phys. A* **13**, 725 (1980).
- [5] Rajarshi Roy, R. Short, J. Durnin, and L. Mandel, "First-passage-time distributions under the influence of quantum fluctuations in a laser," *Phys. Rev. Lett.* **45**, 1486–1490 (1980).
- [6] F. T. Hioe and Surendra Singh, "Correlations, transients, bistability, and phase-transition analogy in two-mode lasers," *Phys. Rev. A* **24**, 2050–2074 (1981).
- [7] P. Lett, W. Christian, Surendra Singh, and L. Mandel, "Macroscopic quantum fluctuations and first-order phase transition in a laser," *Phys. Rev. Lett.* **47**, 1892–1895 (1981).
- [8] Michael J Hartmann, Fernando GSL Brandao, and Martin B Plenio, "Strongly interacting polaritons in coupled arrays of cavities," *Nature Phys.* **2**, 849–855 (2006).
- [9] Andrew D Greentree, Charles Tahan, Jared H Cole, and Lloyd CL Hollenberg, "Quantum phase transitions of light," *Nature Phys.* **2**, 856–861 (2006).
- [10] Dimitris G. Angelakis, Marcelo Franca Santos, and Sougato Bose, "Photon-blockade-induced Mott transitions and XY spin models in coupled cavity arrays," *Phys. Rev. A* **76**, 031805 (2007).
- [11] Alexandre Le Boité, Giuliano Orso, and Cristiano Ciuti, "Steady-state phases and tunneling-induced instabilities in the driven dissipative Bose-Hubbard model," *Phys. Rev. Lett.* **110**, 233601 (2013).
- [12] Ryan M. Wilson, Khan W. Mahmud, Anzi Hu, Alexey V. Gorshkov, Mohammad Hafezi, and Michael Foss-Feig, "Collective phases of strongly interacting cavity photons," *Phys. Rev. A* **94**, 033801 (2016).
- [13] Matteo Biondi, Gianni Blatter, Hakan E Türeci, and Sebastian Schmidt, "Nonequilibrium phase diagram of the driven-dissipative photonic lattice," [arXiv:1611.00697](https://arxiv.org/abs/1611.00697) (2016).
- [14] H. J. Carmichael, "Breakdown of photon blockade: A dissipative quantum phase transition in zero dimensions," *Phys. Rev. X* **5**, 031028 (2015).
- [15] W. Casteels, F. Storme, A. Le Boité, and C. Ciuti, "Power laws in the dynamic hysteresis of quantum nonlinear photonic resonators," *Phys. Rev. A* **93**, 033824 (2016).
- [16] J. J. Mendoza-Arenas, S. R. Clark, S. Felicetti, G. Romero, E. Solano, D. G. Angelakis, and D. Jaksch, "Beyond mean-field bistability in driven-dissipative lattices: Bunching-antibunching transition and quantum simulation," *Phys. Rev. A* **93**, 023821 (2016).
- [17] Wim Casteels, Rosario Fazio, and Cristiano Ciuti, "Critical scaling of the liouvillian gap for a nonlinear driven-dissipative resonator," [arXiv:1608.00717](https://arxiv.org/abs/1608.00717) (2016).
- [18] Michael Foss-Feig, Pradeep Niroula, Jeremy T Young, Mohammad Hafezi, Alexey V Gorshkov, Ryan M Wilson, and Mohammad F Maghrebi, "Emergent equilibrium in many-body optical bistability," [arXiv:1611.02284](https://arxiv.org/abs/1611.02284) (2016).
- [19] E. M. Kessler, G. Giedke, A. Imamoglu, S. F. Yelin, M. D. Lukin, and J. I. Cirac, "Dissipative phase transition in a central spin system," *Phys. Rev. A* **86**, 012116 (2012).
- [20] Arka Majumdar, Armand Rundquist, Michal Bajcsy, Vaishno D. Dasika, Seth R. Bank, and Jelena Vučković, "Design and analysis of photonic crystal coupled cavity arrays for quantum simulation," *Phys. Rev. B* **86**, 195312 (2012).
- [21] Philippe Hamel, Samir Haddadi, Fabrice Raineri, Paul Monnier, Gregoire Beaudoin, Isabelle Sagnes, Ariel Levenson, and Alejandro M Yacomotti, "Spontaneous mirror-symmetry breaking in coupled photonic-crystal nanolasers," *Nature Photon.* **9**, 311–315 (2015).
- [22] Jason W Fleischer, Mordechai Segev, Nikolaos K Efremidis, and Demetrios N Christodoulides, "Observation of two-dimensional discrete solitons in optically induced nonlinear photonic lattices," *Nature* **422**, 147–150 (2003).
- [23] R. Vijay, M. H. Devoret, and I. Siddiqi, "Invited review article: The Josephson bifurcation amplifier," *Rev. Sci. Instrum.* **80**, 111101 (2009).
- [24] D. L. Underwood, W. E. Shanks, Jens Koch, and A. A. Houck, "Low-disorder microwave cavity lattices for quantum simulation with photons," *Phys. Rev. A* **86**, 023837 (2012).
- [25] Matt Eichenfield, Jasper Chan, Ryan M Camacho, Kerry J Vahala, and Oskar Painter, "Optomechanical crystals," *Nature* **462**, 78–82 (2009).
- [26] Eduardo Gil-Santos, Matthieu Labousse, Christophe Baker, Arthur Goetschy, William Hease, Carmen Gomez, Aristide Lemaître, Giuseppe Leo, Cristiano Ciuti, and Ivan Favero, "Light-mediated cascaded locking of multiple nano-optomechanical oscillators," [arXiv:1609.09712](https://arxiv.org/abs/1609.09712) (2016).

- [27] Iacopo Carusotto and Cristiano Ciuti, “Quantum fluids of light,” *Rev. Mod. Phys.* **85**, 299–366 (2013).
- [28] Na Young Kim, Kenichiro Kusudo, Congjun Wu, Naoyuki Masumoto, Andreas Löffler, Sven Höfling, Norio Kumada, Lukas Worschech, Alfred Forchel, and Yoshihisa Yamamoto, “Dynamical d-wave condensation of exciton-polaritons in a two-dimensional square-lattice potential,” *Nat. Phys.* **7**, 681–686 (2011).
- [29] F. Baboux, L. Ge, T. Jacqmin, M. Biondi, E. Galopin, A. Lemaître, L. Le Gratiet, I. Sagnes, S. Schmidt, H. E. Türeci, A. Amo, and J. Bloch, “Bosonic condensation and disorder-induced localization in a flat band,” *Phys. Rev. Lett.* **116**, 066402 (2016).
- [30] Alberto Amo *et al.*, “Superfluidity of polaritons in semiconductor microcavities,” *Nat. Phys.* **5**, 805 (2009).
- [31] A. Baas, J. Ph. Karr, H. Eleuch, and E. Giacobino, “Optical bistability in semiconductor microcavities,” *Phys. Rev. A* **69**, 023809 (2004).
- [32] TK Paraíso, M Wouters, Y Léger, F Morier-Genoud, and B Deveaud-Plédran, “Multistability of a coherent spin ensemble in a semiconductor microcavity,” *Nature Mater.* **9**, 655–660 (2010).
- [1] SRK Rodriguez, A Amo, I Sagnes, L Le Gratiet, E Galopin, A Lemaître, and J Bloch, “Interaction-induced hopping phase in driven-dissipative coupled photonic microcavities,” *Nature Commun.* **7**, 11887 (2016).
- [6] C. N. Luse and A. Zangwill, “Discontinuous scaling of hysteresis losses,” *Phys. Rev. E* **50**, 224–226 (1994).
- [35] Joseph Kerckhoff, Michael A. Armen, and Hideo Mabuchi, “Remnants of semiclassical bistability in the few-photon regime of cavity QED,” *Opt. Express* **19**, 24468–24482 (2011).
- [3] H. Abbaspour, G. Sallen, S. Trebaol, F. Morier-Genoud, M. T. Portella-Oberli, and B. Deveaud, “Effect of a noisy driving field on a bistable polariton system,” *Phys. Rev. B* **92**, 165303 (2015).
- [37] H. M. Gibbs, S. L. McCall, and T. N. C. Venkatesan, “Differential gain and bistability using a sodium-filled Fabry-Perot interferometer,” *Phys. Rev. Lett.* **36**, 1135–1138 (1976).
- [38] A. Dorsel, J. D. McCullen, P. Meystre, E. Vignes, and H. Walther, “Optical bistability and mirror confinement induced by radiation pressure,” *Phys. Rev. Lett.* **51**, 1550–1553 (1983).
- [39] Peter Jung, George Gray, Rajarshi Roy, and Paul Mandel, “Scaling law for dynamical hysteresis,” *Phys. Rev. Lett.* **65**, 1873–1876 (1990).
- [40] G. Rempe, R. J. Thompson, R. J. Brecha, W. D. Lee, and H. J. Kimble, “Optical bistability and photon statistics in cavity quantum electrodynamics,” *Phys. Rev. Lett.* **67**, 1727–1730 (1991).
- [41] L. Collot, V. Lefvre-Seguin, M. Brune, J. M. Raimond, and S. Haroche, “Very high-Q whispering-gallery mode resonances observed on fused silica microspheres,” *EPL (Europhysics Letters)* **23**, 327 (1993).
- [42] Vilson R. Almeida and Michal Lipson, “Optical bistability on a silicon chip,” *Opt. Lett.* **29**, 2387–2389 (2004).
- [43] Masaya Notomi, Akihiko Shinya, Satoshi Mitsugi, Goh Kira, Eiichi Kuramochi, and Takasumi Tanabe, “Optical bistable switching action of Si high-Q photonic-crystal nanocavities,” *Opt. Express* **13**, 2678–2687 (2005).
- [44] G. A. Wurtz, R. Pollard, and A. V. Zayats, “Optical bistability in nonlinear surface-plasmon polaritonic crystals,” *Phys. Rev. Lett.* **97**, 057402 (2006).
- [45] T. Boulier *et al.*, “Polariton-generated intensity squeezing in semiconductor micropillars,” *Nature Commun.* **5** (2014).
- [46] H. Risken, C. Savage, F. Haake, and D. F. Walls, “Quantum tunneling in dispersive optical bistability,” *Phys. Rev. A* **35**, 1729–1739 (1987).
- [47] K. Vogel and H. Risken, “Quantum-tunneling rates and stationary solutions in dispersive optical bistability,” *Phys. Rev. A* **38**, 2409–2422 (1988).
- [48] Mark Dykman, *Fluctuating nonlinear oscillators: from nanomechanics to quantum superconducting circuits* (OUP Oxford, 2012).
- [49] See Supplemental Material for details about the sample, setup characterization, noise measurements, mean-field calculations, scaling analysis, estimates of the polariton-polariton interaction constant in different micropillars, and comparison between measurements and calculations.
- [50] Jacek Dziarmaga, “Dynamics of a quantum phase transition and relaxation to a steady state,” *Adv. Phys.* **59**, 1063–1189 (2010).
- [51] T. Jacqmin, I. Carusotto, I. Sagnes, M. Abbarchi, D. D. Solnyshkov, G. Malpuech, E. Galopin, A. Lemaître, J. Bloch, and A. Amo, “Direct observation of Dirac cones and a flatband in a honeycomb lattice for polaritons,” *Phys. Rev. Lett.* **112**, 116402 (2014).
- [52] V. G. Sala, D. D. Solnyshkov, I. Carusotto, T. Jacqmin, A. Lemaître, H. Tercas, A. Nalitov, M. Abbarchi, E. Galopin, I. Sagnes, J. Bloch, G. Malpuech, and A. Amo, “Spin-orbit coupling for photons and polaritons in microstructures,” *Phys. Rev. X* **5**, 011034 (2015).
- [53] D. Tanese, E. Gurevich, F. Baboux, T. Jacqmin, A. Lemaître, E. Galopin, I. Sagnes, A. Amo, J. Bloch, and E. Akkermans, “Fractal energy spectrum of a polariton gas in a fibonacci quasiperiodic potential,” *Phys. Rev. Lett.* **112**, 146404 (2014).
- [54] E. Akkermans, G. V. Dunne, and A. Teplyaev, “Physical consequences of complex dimensions of fractals,” *EPL (Europhysics Letters)* **88**, 40007 (2009).
- [55] Eric Akkermans, Gerald V. Dunne, and Alexander Teplyaev, “Thermodynamics of photons on fractals,” *Phys. Rev. Lett.* **105**, 230407 (2010).

SUPPLEMENTAL MATERIAL

Sample details

The planar cavity was grown by molecular beam epitaxy and comprises a GaAs λ cavity between two $\text{Ga}_{0.9}\text{Al}_{0.1}\text{As}/\text{Ga}_{0.05}\text{Al}_{0.95}\text{As}$ distributed Bragg reflectors with 26 and 30 pairs of layers at the top and bottom, respectively. One 80 Å-wide $\text{In}_{0.04}\text{Ga}_{0.96}\text{As}$ quantum well is positioned at the center of the cavity. A Rabi splitting of 3.4 meV results from strong exciton-photon coupling. The three rectangular micropillars (all having 2:1 aspect ratio) were fabricated by electron beam lithography and dry etching of the planar cavity. With reference to the labels in Fig. 4(a) of the main manuscript, the cross-sectional area A_c of the micropillars are: $A_c = 6 \mu\text{m}^2$ for cavity 1, $A_c = 8 \mu\text{m}^2$ for cavity 2, and $A_c = 29 \mu\text{m}^2$ for cavity 3.

Retrieval of parameters

The mode frequency ω_0 and polariton loss rate γ of each micropillar were deduced by measuring the transmitted spectrum under weak driving ($< 1 \mu\text{W}$), and fitting a Lorentzian lineshape as shown in Fig. 1(b) of the main manuscript. The polariton-polariton interaction energy U of each micropillar was estimated following the procedure described in detail in Ref. 1, and which we summarize below. To begin, we took the exciton-exciton interaction constant to be $g_{\text{exc}} = 30 \mu\text{eV} \cdot \mu\text{m}^2$. This value is consistent with theoretical predictions [2] and with our previous observations [1]. Next, we calculated the 2D polariton-polariton interaction constant as $U_{2\text{D}} = g_{\text{exc}}|X|^4$, with $|X|^2$ the exciton fraction of the polariton admixture. To obtain the value of $|X|^2$ as a function of energy, we analyzed the exciton-polariton dispersion in an effectively 2D cavity adjacent to the micropillars in the wafer. In particular, we fitted the eigenvalues of a 2×2 Hamiltonian to the polariton dispersion, and obtained $|X|^2$ from the eigenvector associated with the lower polariton eigenvalue (energy). We then evaluated the value of $|X|^2$ at the energy of each micropillar mode to calculate $U_{2\text{D}}$. Finally, using the cross-sectional area of each micropillar A_c , we obtain $U = U_{2\text{D}}/A_c$.

The retrieved parameters are:

- i) For the cavity under study in all figures of the main manuscript [cavity 2 in Fig. 4(a)], we have $\hbar\omega_0 = 1478.687 \pm 0.004 \text{ meV}$, $\gamma = 31 \pm 2 \mu\text{eV}$, $|X|^2 = 0.13$, and $U/\gamma = 2_{-1.6}^{+8} \cdot 10^{-3}$.
- ii) For cavity 1 in Fig. 4(a) of the main manuscript, we have $\hbar\omega_0 = 1479.695 \pm 0.004 \text{ meV}$, $\gamma = 31 \pm 3 \mu\text{eV}$, $|X|^2 = 0.21$, and $U/\gamma = 1_{-0.8}^{+4} \cdot 10^{-2}$.
- iii) For cavity 3 in Fig. 4(a) of the main manuscript, we have $\hbar\omega_0 = 1472.752 \pm 0.004 \text{ meV}$, $\gamma = 30 \pm 2 \mu\text{eV}$, $|X|^2 = 0.02$, and $U/\gamma = 2_{-1.6}^{+8} \cdot 10^{-5}$.

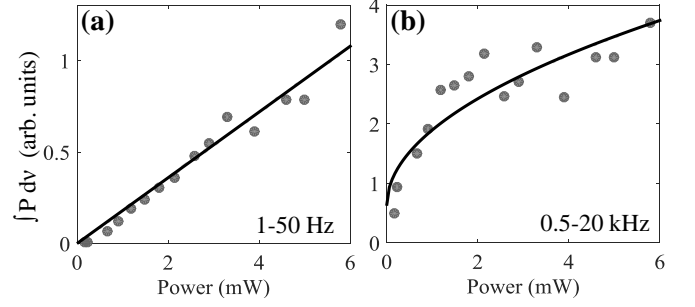


FIG. 5. Power-dependence of the noise in the driving laser integrated over the frequency range indicated in each panel. The black line in (a) is a linear fit, and the black line in (b) is a square root fit. The square root behavior at high frequencies is indicative of shot noise.

Measurement details

The driving laser is a tunable MSquare Ti:Sapphire oscillator with a linewidth below 10 MHz. The laser frequency is locked with an accuracy of 0.1 pm. Given the typical values of γ and $\hbar\omega_0$ (see above), this translates to an uncertainty in Δ/γ on the order of ± 0.01 . The excitation and collection objectives have a numerical aperture of 0.5 and 0.4, respectively. For all three cavities the excitation laser beam is linearly polarized parallel to the long axis of the rectangular micropillars, thereby probing the lowest energy mode. For the cavity under study in all figures of the main text, the lowest energy mode for the orthogonal polarization (along the short axis) is $\sim 5\gamma$ higher in energy, while co-polarized higher energy states are several tens of γ away. Thus, the single mode approximation holds reasonably well.

To verify that our dynamic hysteresis measurements were shot-noise limited, we analyzed the power spectral density of the driving laser. The laser beam passed through our entire optical setup to reproduce the experimental conditions of the dynamic hysteresis measurements. At low frequencies (1- 50 Hz), where various fluctuations are significant, Fig. 5(a) shows that the noise power scales linearly with the total power. In contrast, at higher frequencies Fig. 5(b) shows that the noise power scales with the square root of the total power, as expected for shot noise. We also observed a frequency-independent noise power spectral density (characteristic of shot noise) in the frequency range of Fig. 5(b). In addition, we note that the power in the modulated signal of our dynamic hysteresis measurements exceeds the noise level by more than four orders of magnitude.

Noise sources

Additional sources of noise (besides shot noise) could also induce switching between metastable states. For instance, in Ref. 3 a large amount of noise was deliberately added to the driving laser to trigger switching between

the two metastable states. In addition, noise could be generated within the cavity. For example, the intracavity polariton field could be subjected to fluctuations linked to acoustic phonon scattering or two photon absorption. In our experiments, phonon scattering can be excluded because kT is much smaller than the energy difference between the state we probe and the next confined polariton state. Fluctuations induced by two photon absorption can be ruled out considering the experiments reported in Fig. 4(a). When probing smaller values of U/γ for fixed Δ/γ , the driving intensity at the critical point is larger. Stronger driving is expected to make two-photon absorption more relevant and thereby reduce the hysteresis area. However, the opposite behavior is observed and we can therefore neglect additional fluctuations induced within the cavity. Thus, we can safely consider that shot noise is the only relevant source of noise in our experiments.

Mean-field calculation details

For the dynamic hysteresis calculations, we consider a triangular modulation of the drive intensity consisting of a linear sweep from I_0 to $I_0 + P_s$ followed by the reverse one from $I_0 + P_s$ back to I_0 :

$$I(t) = I_0 + \frac{t}{t_s} P_s \theta(t_s - t) - \frac{t - 2t_s}{t_s} P_s \theta(t - t_s), \quad (4)$$

Here, P_s is the range of the power sweep, t_s is the scanning time, and the effective sweep velocity is P_s/t_s . Introducing the sweep (4) in the equation of motion for the mean-field α (see main manuscript) with $t_s/P_s = 10^6/(5\gamma^3) = 2.1 \cdot 10^{-5} \text{ s}/\mu\text{W}$ leads to the dynamic hysteresis presented in Fig. 2(d) of the main manuscript.

Scaling Analysis

In general, a master equation can be defined in terms of its Liouvillian superoperator $\hat{\mathcal{L}}$, namely $\partial_t \hat{\rho} = \hat{\mathcal{L}} \hat{\rho}$. The Liouvillian superoperator has a complex spectrum of eigenvalues λ . Their imaginary part has the meaning of an excitation frequency, while their real part determines the dissipation rate. The steady-state density matrix $\hat{\rho}_{ss}$ corresponds to the eigenvector of $\hat{\mathcal{L}}$ with eigenvalue $\lambda = 0$, namely $\hat{\mathcal{L}} \hat{\rho}_{ss} = 0$. The dynamical properties depend on the non-zero complex eigenvalues. The Liouvillian gap $\bar{\lambda}$ is defined as the non-zero eigenvalue of $\hat{\mathcal{L}}$ with real part closest to zero. In general, the Liouvillian gap becomes highly suppressed as a system enters a critical region [4]. This leads to a critical slowing down of the dynamics, and a dissipative phase transition when the gap $\bar{\lambda}$ closes. Around the bistability the imaginary part of $\bar{\lambda}$ is strictly zero and $|\text{Re} \bar{\lambda}|$ exhibits a minimum at a driving intensity in the midst of the bistability region [5]. From the real part of $\bar{\lambda}$ the reaction time τ_R can be determined as: $\tau_R = 1/|\text{Re} \bar{\lambda}|$. τ_R corresponds to the longest timescale on which the system relaxes to its

steady-state. The transition point is defined as the intensity I_t where τ_R reaches the maximal value τ_{tunn} , the tunneling time.

A consequence of the above behavior of the Liouvillian gap is that the system can respond non-adiabatically when the driving power is varied across the optical bistability region. The sweep timescale τ_S is defined by the inverse normalised transition rate of the sweep (4): $\tau_S = |\dot{\epsilon}/\epsilon|^{-1}$, where ϵ is the distance from the transition point: $\epsilon = I(t) - I_t$. The non-adiabatic range is reached when the sweep timescale τ_S is smaller than the system reaction time τ_R , i.e. for $\tau_S < \tau_R$. If this condition is fulfilled, the system can not relax to its steady-state and a dynamic hysteresis arises. The point where the system enters or exits this non-adiabatic regime can be estimated by equating the two timescales: $\tau_S = \tau_R$. This allows to determine the size of the non-adiabatic range δI , as indicated by the blue dashed lines in the inset of Fig. 3(b) of the main manuscript for $U = 0.0075\gamma$ and $\Delta = \gamma$. Reference [5] showed that δI exhibits the same double power-law scaling as the hysteresis area. Moreover, in the slow sweep limit the prefactor of the power law with exponent -1 is directly related to the tunneling time: $\delta I = 2\tau_{\text{tunn}} P_s/t_s$. The above scaling analysis was used to calculate the results in Fig. 3(b) and Fig. 4(b) of the main manuscript.

Comparing measurements and calculations

A quantitative comparison between experiments and calculations requires a precise knowledge of the experimental excitation efficiency. This is needed to compare driving powers. Since excitation through the cryostat makes it difficult to know the excitation efficiency exactly, we deduced it by requiring that the theoretical range where the transition occurs in Fig. 1(c) of the main manuscript corresponds to the experimental one observed in Fig. 2(d). With this approach, we deduced a conversion factor of 0.75 between the theoretical units of γ^2 for the driving intensity and the experimentally measured power in μW , i.e.: $I[\gamma^2] = 0.75 \text{ Power} [\mu\text{W}]$.

The values of U/γ used in the calculations in Fig. 3(b) and Fig. 4(b) of the main manuscript were adjusted with respect to the corresponding estimates for the experimental cavities (see above). For the calculations corresponding to cavity 1 and cavity 2, we took the experimentally estimated value of U/γ times a factor of 0.4 and 3.5, respectively. Note that the adjusted values are within the experimental uncertainties given above. These adjustments were only done to match the measured time of the transition to the power law with exponent -1 , and they do not affect in any way the retrieved exponents. For cavity 3, the estimated $U/\gamma = 2_{-1.6}^{+8} \cdot 10^{-5}$ was replaced by the value $U/\gamma = 0.002$ in the calculations. This modification is due to the extremely small experimental value of U/γ being beyond our computational capabilities. Despite this seemingly large adjustment of U/γ ,

both experimental and theoretical curves follow a single power law within the observation window because fluctuations are largely irrelevant to the dynamics given the large average photon number in cavity 3.

In the caption of Fig. 4 we also mention that some of the curves were multiplied by a constant factor (given in the caption) simply for improving the clarity of the figure. These multiplications were only done to improve the visibility of details in the data given the finite space for the figure. These multiplications do not affect in any way the retrieved exponents, nor do they affect the critical times of the transition from one power law to another; they only shift the curves down or up in the log scale.

Finally, we would like to mention that a double power law decay of the hysteresis area could also be observed when a nonlinear system is subjected to thermal (or other) fluctuations. However, the exponents and critical times can depend on the details of the system. For instance, Luse and Zangwill calculated different exponents for several mean-field treatments of the kinetic Ising model [6]. In our optical experiments, where laser

shot is the only relevant source of fluctuations, the measured exponents are in good agreement with calculations including quantum fluctuations only.

* said.rodriquez@lpn.cnrs.fr

- [1] S. Rodriguez, A. Amo, I. Sagnes, L. Le Gratiet, E. Galopin, A. Lemaitre, and J. Bloch, *Nature Commun.* **7**, 11887 (2016).
- [2] C. Ciuti, V. Savona, C. Piermarocchi, A. Quattropani, and P. Schwendimann, *Phys. Rev. B* **58**, 7926 (1998).
- [3] H. Abbaspour, G. Sallen, S. Trebaol, F. Morier-Genoud, M. T. Portella-Oberli, and B. Deveaud, *Phys. Rev. B* **92**, 165303 (2015).
- [4] E. M. Kessler, G. Giedke, A. Imamoglu, S. F. Yelin, M. D. Lukin, and J. I. Cirac, *Phys. Rev. A* **86**, 012116 (2012).
- [5] W. Casteels, F. Storme, A. Le Boité, and C. Ciuti, *Phys. Rev. A* **93**, 033824 (2016).
- [6] C. N. Luse and A. Zangwill, *Phys. Rev. E* **50**, 224 (1994).